Journal of Thermal Science Vol.31, No.5 (2022) 1663−1681

https://doi.org/10.1007/s11630-022-1611-z **Article ID: 1003-2169(2022)05-1663-19**

Simulation of Combustion Flow of Methane Gas in a Premixed Low-Swirl Burner using a Partially Premixed Combustion Model

XIAO Caiyuan[1,2*], OMIDI Milad[3], SURENDAR A.[4], ALIZADEH As'ad[5,6], BOKOV Dmitry O.[7], BINYAMIN[8], TOGHRAIE Davood[3*]

1. Key Laboratory of Hunan Province for Efficient Power System and Intelligent Manufacturing, Shaoyang 422000, China
2. College of Mechanical and Energy Engineering, Shaoyang University, Shaoyang 422000, China
3. Department of Mechanical Engineering, Khomeinishahr Branch, Islamic Azad University, Khomeinishahr 119/84175, Iran
4. Department of Pharmacology, Saveetha dental College and hospital, Saveetha institute of medical and technical sciences, Chennai 602105, India
5. Faculty of Engineering, Soran University, Soran 651, Iraq
6. Department of Mechanical Engineering, College of Engineering, University of Zakho, Zakho 1653654, Iraq
7. Institute of Pharmacy, Sechenov First Moscow State Medical University, Moscow 119991, Russian Federation
8. Department of Mechanical Engineering, Faculty of Science and Technology, Universitas Muhammadiyah Kalimantan Timur, Samarinda 75124, Indonesia

Abstract: Because the rotational current stabilizes the flame by creating a recirculation zone, it may increase the risk of reversal. For this reason, low-spin combustion is used to stabilize the flame while preventing flashbacks. Therefore, in this study, the combustion flow of methane gas in a low-swirl burner is simulated using a partially premixed combustion model. Furthermore, the fuel flow rate is considered constant. The research parameters include swirl angle (θ=35°–47°), equivalence ratio (φ=0.6–0.9) and inlet axial flow radius (R=0.6–0.7) and effect of these parameters on temperature distribution, flame length, flame rise length, velocity field, and streamlines of the number of pollutant species are investigated. The contours of streamline, temperature distribution, and velocity distribution are also presented for analysis of flow physics. The results show that with increasing the fuel-air ratio, the strength of the axial flow decreases, and the position of the maximum flame temperature shifts toward the inlet of the reactants. The results also reveal that by increasing the swirl angle of the flow, the position of the minimum velocity value (opposite to the direction of the axis) tends towards the outlet. The results also indicate that the maximum temperature of the combustion chamber increases with increasing the swirl angle, and in θ=35°, the maximum temperature is 1711°C and in θ=41°, this value is 1812°C. Finally, by increasing the swirl angle to θ=47°, the maximum flame temperature position is found at a considerable distance from the inlet and is 1842°C.

Keywords: swirl burner, numerical simulation, axial velocity, premixed combustion, V-shaped flame

Received: Nov 30, 2021 Corresponding author: XIAO Caiyuan; E-mail: Caiyuanxiao@iaukhsh.ac.ir; xiaocaiyuan1999@163.com
AE: YANG Bin TOGHRAIE Davood Toghraee@iaukhsh.ac.ir

1. Introduction

As a result of the development of human science, the ever-growing need for energy, and reduced fossil resources, high-efficiency combustion devices are increasingly demanded. Although many attempts have been made to find alternative energy sources, combustion is still widely used for energy production in the industry. Consequently, optimizing the emerging combustion equipment, including different burners, has been considerably considered. In this regard, the use of the swirling flow has been proposed as one of the valuable solutions. The swirling combustion is commonly used for sustainable and efficient combustion in industrial furnaces, boilers, gas turbines with swirling areas, and internal combustion engines [1–3]. Extensive research on combustion swirling flows is classified into experimental and numerical studies [4, 5]. The research parameters include air-fuel ratio, non-premixed air-fuel velocity ratio, premixed air-fuel mixture velocity, swirling rate, the stability range of different flame regimes, burner geometry, and the rate of combustion pollutants formation [6].

So far, various studies have been conducted in the field of rotating flames. For example, Kamal et al. [7] examined pulverized coal/premixed gas/air streams' co-firing in a double Swirl Combustor. The results showed that the mixture of these substances leads to earlier contact with air and delays the NO_x reduction mechanism. Kashkousha et al. [7] examined the reverse diffusion and semi-premixed flames in different ellipse/rotation and cross currents. The results revealed that by changing the relative angular direction of the nozzle, the combustion performance could be controlled. Azam et al. [8] examined the combustion performance of triple flames. These flames were considered to be caused by elliptical and circular rotations. The results revealed that the elliptical rotation of the shorter flame length had a lower NO_x emission than the circular rotation. Fahmy et al. [9] examined the combustion performance of elliptical rotations. The results revealed that increasing the secondary rotation angle reduces the emission of pollutants. Mohy et al. [10] examined the flow of fuel and air in elliptical and darya rotation. The results revealed that the flame is significantly shorter in elliptical rotation.

On the other hand, in the field of low swirl combustion (LSB), Cheng is the pioneer [11]. He and his research team did a lot of research in this area. For instance, they investigated the hydrodynamic effect of scale reduction on flow field evolution in an LSB burner [12]. Using PIV, three different rotors from 12 mm to 25.4 mm were studied, showing an output range of less than 1 kW to more than 23 kW. The emission results from a 14 mm diameter LSB burner with an output of 3.33 kW proved the system's feasibility in a sufficiently lean mixture. Also, the integration of the newly developed LSB into a can-style combustion chamber for microturbine applications was completed and easily met the precise emission targets. In another study, they examined the capability of LSB for commercial and industrial furnaces and boilers [13]. They revealed that NO_x emission is a function of equivalence ratio and is independent of thermal input. In a study, Zhao et al. [14] conducted a numerical and experimental study of the rotational flow in gas turbine burners to improve the uniformity of fuel/air mixing and to stabilize non-fat premixed flames. They used a laser Doppler accelerometer (LDV) and particle image accelerometer (PIV) to evaluate reaction field properties. Their results showed that burners with better mixing performance had a homogeneous reaction field with less turbulence and NO_x emissions of 2.5×10^{-6} ($15\%O_2$). Linden [15] conducted a study on swirling flow, analyzed the effect of geometric parameters on separation efficiency in industrial separators and concluded that the change in geometric parameters significantly changes the separation efficiency of industrial separators. Early studies on the swirling flow combustion were conducted by Beer and Miklós [16]. They realized that the velocity distribution is Gaussian in a weak swirl. Most of the studies focus on the swirl combustion chamber and the effect of swirl on NO_x formation, which was first addressed by Claypole and Syred [17]. They showed that increasing swirl played a major role in reducing NO_x emissions. Buckley et al. [18] dealt with the effect of different swirls on the efficiency of a combustion chamber and the pollutant formation. The results revealed that the use of swirl reduces NO_x and CO and simultaneously increases the efficiency of the combustion chamber. Cho et al. [19] considered the improvement of flame stability and NO_x reduction in lean premixed combustion by adding hydrogen and showed that in lean premixed combustion, flames are unstable because combustion occurs near the lower flammability limit.

Tummers et al. [20] formed a V-shaped flame, compared it with ordinary flames, and observed that intense recirculation of combustion products, driven by strong reverse flow, provides a hot core as a source of stabilization, causes pre-heating of air and fuel, and enhances their mixing. Visual flame length decreases by a factor of three, and the compact flame shows a broader range of parameters to operate in a stable regime. Zhao et al. [21] evaluated the thermal efficiency of a premixed swirl burner and indicated that swirling leads to better combustion and higher thermal efficiency. Paubel et al. [22] investigated flame stability diagrams for three types

of non-premixed oxygen, residual gas combustion with low calorific value (In Type 1, two concentric flames are attached at the burner nozzle. In Type 2, the internal blast furnace gases (BFG) flame is lifted. In Type 3, a single annulus flame burning a fuel mixture of CH_4 and BFG with the external oxygen). The results indicated that using methane-pure oxygen flame leads to burning residual gases with low calorific value in a wide range of operating conditions. Hashemi et al. [23] also carried out another study and obtained the maximum radiation of the burner is obtained at the maximum firing rate in the range of equivalence ratio (φ=0.8–1). Jin et al. [24] dealt with the stability of premixed flames by the opposite jet to stabilize the flame in high-velocity combustible streams such as in ramjet and afterburner. Ciani et al. [25] carried out an experimental analysis of the stability of diffusion and stability diagrams for N_2-diluted methane/air flames in a burner with an opposite jet. They demonstrated that the flame could deform in the region of instability by increasing or decreasing the strain rate. Raghavan et al. [26] in an experimental study of a flat plate premixed burner, investigated the combustion parameters affecting the flame and found by reducing the equivalence ratio, the premix flame stability increases, and also the multi-hole matrix plate burner is more efficient than a conventional large size single burner burner due to less pollutant emissions. They simulated the combustion of a multi-hole flat cylindrical premix with natural liquefied petroleum gas and observed that the presence of a retaining hole increases stability and the flammability limit.

Other studies such as Kerr et al. [27], Mathur et al. [28] ,Yuasa [29], Gupta et al. [30], Feikema et al. [31], Choi and Kim [32], Cavaliere et al. [33], Heeger et al. [34], Kwark et al. [35], Kotani and Takeno [36], Chao et al. [37], Lee et al. [38], Diamantis et al. [39], Hashemi et al. [40, 41], Lee et al. [42], etc. have also been done. This review of the literature indicates that most of the research has focused on the stability range of the flame regime, the geometry of the burner, the rate of swirling, and the calculation of the rate of combustion pollutants. Also, the effect of air to fuel ratio, rotation angle applied on the rotating blower on field characteristics, flow, temperature, and pollutant production have been investigated in these studies [43–46]. Therefore, the innovation of the present study is to analyze the effect of equivalence ratios and swirl angles of different flows as well as changing the inlet radius of the axial flow on the stability of the flame.

2. Governing Equations and Solution Method

2.1 Statement of the problem

In the present study, the combustion flow of methane in a low-swirl burner is simulated using the finite volume method (FVM) and ANSYS FLUENT software. The SIMPLE algorithm is used to account for the pressure-velocity coupling and solve other equations such as momentum, pressure, energy, and volume fraction, the second-order upwind scheme. The schematic of the burner geometry under consideration is shown in Fig. 1.

Steady, turbulent, and three-dimensional flows are considered as the operating conditions. The 3D geometry is symmetrical about its axis. Therefore, the geometry is considered two-dimensional, and the flow and heat transfer fields are simulated using an asymmetric axial solver.

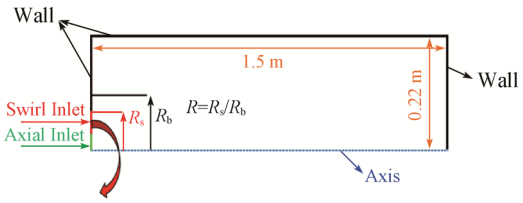

Fig. 1 Schematic of the geometry under consideration in the present study

2.2 Simulation of premixed low swirl combustion

A partially premixed model combines premixed and non-premixed combustion models in the present study. The ECFM is employed to model the premixed combustion. The ECFM is a modified model of the *c*-equation and *G*-equation premixed models. In the *c*-model, a scalar variable that determines the reaction propagation from burned to unburned categories is denoted by *c*. The transfer equation for *c* indicates the spatial variation of the reaction propagation in the turbulent flow field. In front of the flame where unburned reactants are present, *c* is zero, and in front of the flame where burnt products are present, *c* is equal to 1. Inside the flame, *c* also changes between 0 and 1. The flame front propagation is determined by solving the transfer equation for the propagation variable averaged by the density $\overline{c}$:

$$\nabla\left(\rho\overline{vc}\right)=\nabla\left[\left(\frac{k}{c_p}+\frac{\mu_t}{Sc_t}\nabla\overline{f}\right)\nabla\overline{c}\right]+\rho S_e \tag{1}$$

where $\overline{c}$ is the mean propagation variable; Sc_t is the turbulent Schmidt number; S_c is the spring expression; k is the thermal conductivity of the mixture, and c_p is the specific heat of the mixture. The propagation variable is defined as follows:

$$c=\frac{\sum_k a_k\left(Y_k-Y_k^{\mathrm{U}}\right)}{\sum_k a_k\left(Y_k^{\mathrm{eq}}-Y_k^{\mathrm{U}}\right)} \tag{2}$$

where U denotes the unburned reactants, and the eq

denotes chemical equilibrium; Y_k denotes the mass fraction of kth and a_k denotes on a constant value. Compared to the c model, in the ECFM an additional transfer equation is solved for the flame area density Σ:

$$\frac{\partial \Sigma}{\partial t}+\nabla\left[\left(\frac{k}{c_p}+\frac{\mu_t}{Sc_t}\nabla\bar{f}\right)\nabla\left(\frac{\Sigma}{\rho}\right)\right] +\left(P_1+P_2+P_3\right)\Sigma+P_4-D \tag{3}$$

where Σ is the density of the flame area; P_1 to P_4 are also the source expressions of the turbulence interactions, flame stretch, diffusion of burnt gases, and the spring expression due to the flame propagation. D is also the scatter of the flame area. The mixture fraction f is the mass fraction formed by the fuel flow, which is expressed as follows [32]:

$$f=\frac{z_i-z_{i-\mathrm{ox}}}{z_{i-\mathrm{fuel}}-z_{i-\mathrm{ox}}} \tag{4}$$

where z_i is the mass fraction of element i; the ox is the value in the inlet oxidizer flow, and the fuel is the value in the inlet fuel flow. Assuming the same diffusion, the equations of the species are reduced to one equation for the mixture fraction f. the density-based average of the mixture fraction is calculated as follows:

$$\frac{\partial}{\partial t}\left(\rho\bar{f}\right)+\nabla\left(\rho\bar{v}\bar{f}\right)=\left[\nabla\left(\frac{\mu_t}{\sigma_t}\nabla\bar{f}\right)\right]+S_m+S_{\mathrm{user}} \tag{5}$$

where the source expression S_m results from transferring mass from liquid fuel droplets or reactive particles (such as soot) into the gas phase. In the previous solution method, in addition to solving the Favre average of the mixture fraction, a conservation equation for the changes in mixture fraction $\overline{f'^2}$ is also solved [32]:

$$\frac{\partial}{\partial t}\left(\rho\overline{f^2}\right)+\nabla\left(\rho\bar{v}\overline{f'^2}\right)=\nabla\left(\frac{\mu_t}{\sigma_t}\nabla\overline{f^2}\right) +C_d\rho\frac{\in}{k}\overline{f'^2}+S_{\mathrm{user}}+S_{\mathrm{user}} \tag{6}$$

where $f'=f-\bar{f}$, σ_t, and C_d are constants with values of 0.85, 2.86 and 2. [32].

2.3 Solution method

The governing equations are used by considering the following conditions:

(1) The flow is single-phase flow, incompressible and turbulent.

(2) Fluid flow and heat transfer are steady and axisymmetric.

At the inlet, the flow rate boundary condition is considered, and at the outlet, the pressure is equal to the surrounding pressure. Assuming the no-slip boundary condition and insulation, the burner walls are modelled. Second-order accuracy is used to solve all equations. The convergence criterion is considered to be 10^{-6} for all equations. In all simulations, the pressure-based solver is employed to solve the equations. The axis velocity at the inlet, adjacent to the axis of symmetry, is included in the computational domain only at the axial velocity but the swirling inlet with the angle of swirling is applied to the radial component of velocity.

2.4 Grid independency

Due to the problem, a structured mesh is used where the minimum element size is 1 mm. Fig. 2 shows the computational mesh. Here, due to the high-temperature gradient on the outlet side of the fuel-air mixture, the mesh density is higher near it. For this purpose, simulations are performed on the number of different elements and the axial temperature distribution obtained in the number of elements shown in Fig. 3. Here, with increasing the number of elements from 60 000 to 110 000, the resulting error is 11%; however, with increasing the number of elements to 200 000, there is no significant change in axial temperature compared to the number of 110 000 elements, and there is a changeless than 3% in temperature with the increasing of the number of elements from 110 000 to 200 000. Therefore, the numerical results obtained in the number of 110 000 elements are independent of the number of elements. As a result, the same number of elements is used in all cases.

2.5 Validation

To validate the numerical solution process, the obtained results are compared with the experimental results in Ebrahim et al. [43]. The flame resulting from methane, hydrogen, and air in swirling conditions was investigated. Fig. 4 shows the axial temperature distribution obtained from numerical simulation with the results presented in Ebrahim et al. [43]. Here, the obtained results are consistent with the experimental results, and the maximum error is 9.5%. The validation shows that the combustion model and the numerical solution method have acceptable accuracy in the present study.

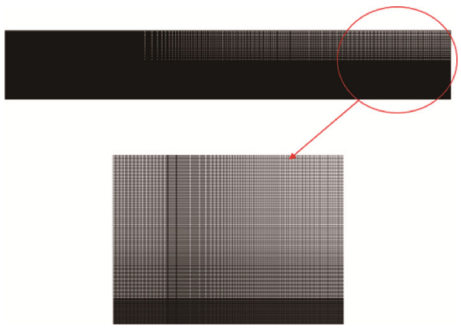

Fig. 2 Computational mesh in the present study

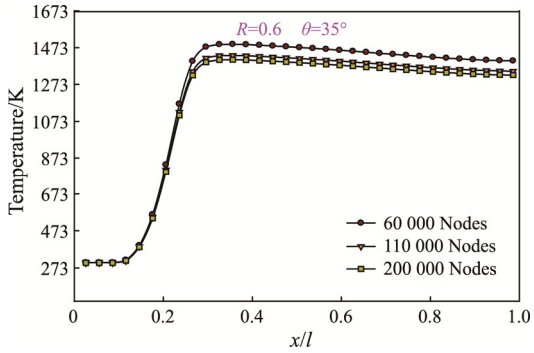

Fig. 3 The grid independence for axial temperature distribution

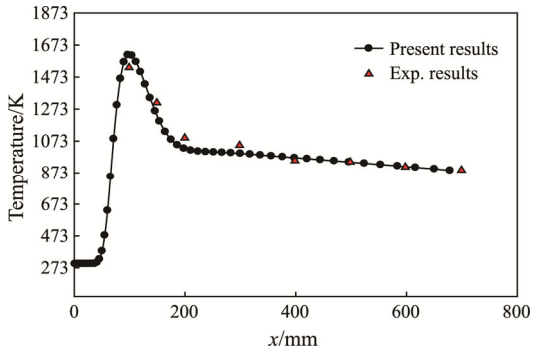

Fig. 4 Axial temperature distribution, comparison of numerical and experimental results of Ref. [43]

3. Results and Discussion

3.1 Effect of equivalence ratio with θ=35°, R=0.6

The obtained results are reported for the conditions in which 60% of the inlet cross-section of the fuel-air mixture enters the burner with axial velocity, and 40% of the inlet cross-section has a swirl velocity and θ=35°. In Fig. 5, the contour of temperature distribution and Fig. 6, the contours of distribution of fourth power temperature are shown in four equivalence ratios. Here, when the mixture of fuel and air is dilute, and φ=0.6, the shape of the flame is different from the other conditions, and the length of the fourth power temperature distribution lines is much higher than the other conditions. The results indicate that with increasing the equivalence ratio and approaching the stoichiometric conditions, a V-shape flame is formed, and the maximum temperature tends towards the outlet of the reactors. Analysis of the maximum temperature shows that with increasing the fuel-air ratio, the flame temperature increases so that at φ=0.6, the maximum temperature is 1458 K and when φ=0.9, the maximum temperature is 1954 K. Establishing a flame with a lower equivalence ratio (more diluted mixture) is important because the burner walls are less damaged. The number of pollutant species decreases, which is one of the advantages of low swirl flames.

Fig. 7 and Fig. 8 show the counters of velocity distribution and streamlines. Here, the maximum axial velocity is 10.4 m/s at φ=0.6, and as the equivalence ratio increases to φ=0.9, the maximum axial velocity reaches 8.4 m/s. Analysis of streamlines indicates that two external vortices and an internal vortex are constantly formed, which are named according to their position inside and outside the flame. The axial outlet flow is diverged due to a radial flow adjacent to the wall, and the amount of this divergence increases with an increasing fuel-to-air ratio. Therefore, the power of the swirling flow is reduced, and the flow becomes fully axial again. By forming an internal vortex, this divergence in velocity

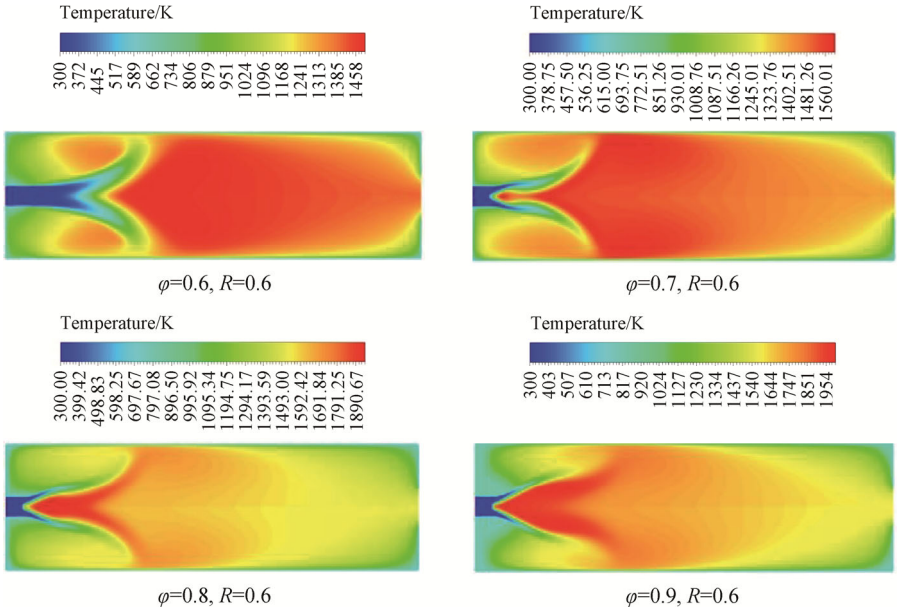

Fig. 5 The contour of temperature distribution at different equivalence ratios, R=0.6 and θ=35°

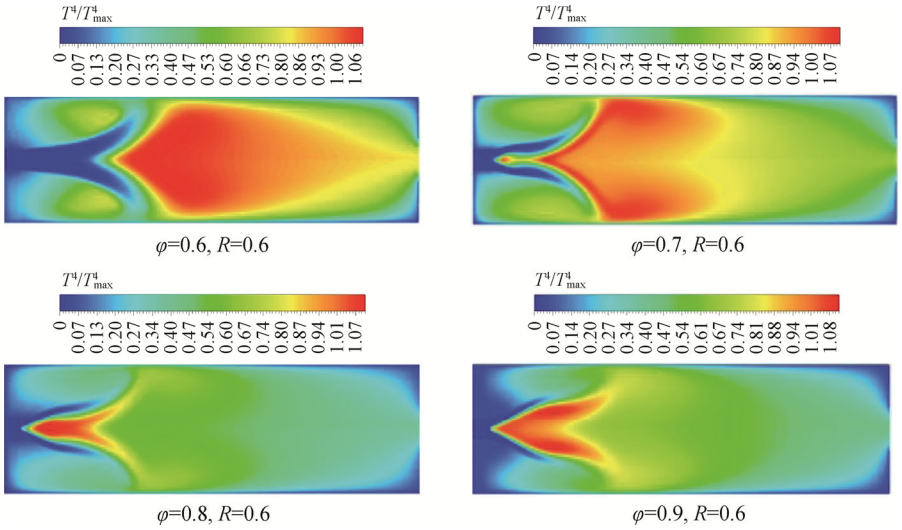

Fig. 6 The contour of the distribution of fourth power temperature (flame shape) at different equivalence ratios, R= 0.6 and θ=35°

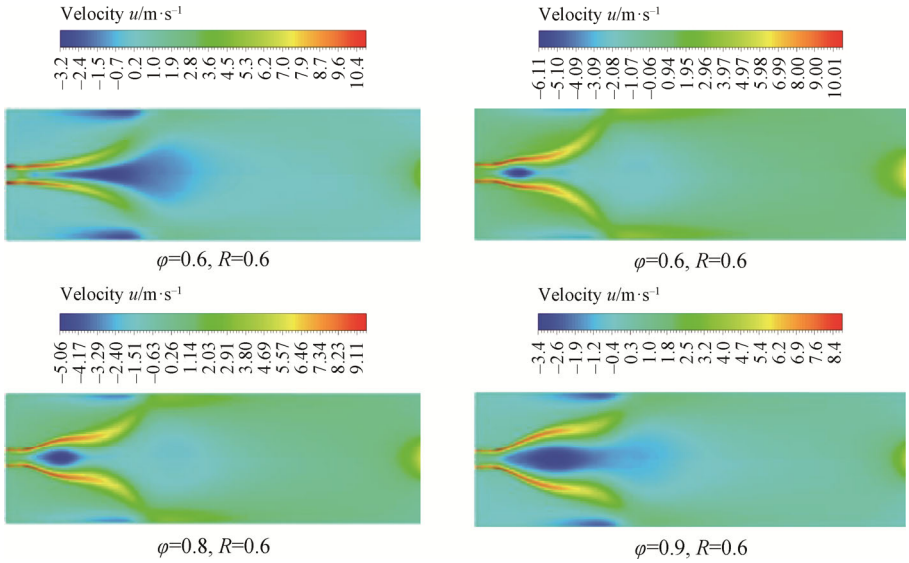

Fig. 7 The contour of axial velocity distribution at different equivalence ratios, R=0.6 and θ=35°

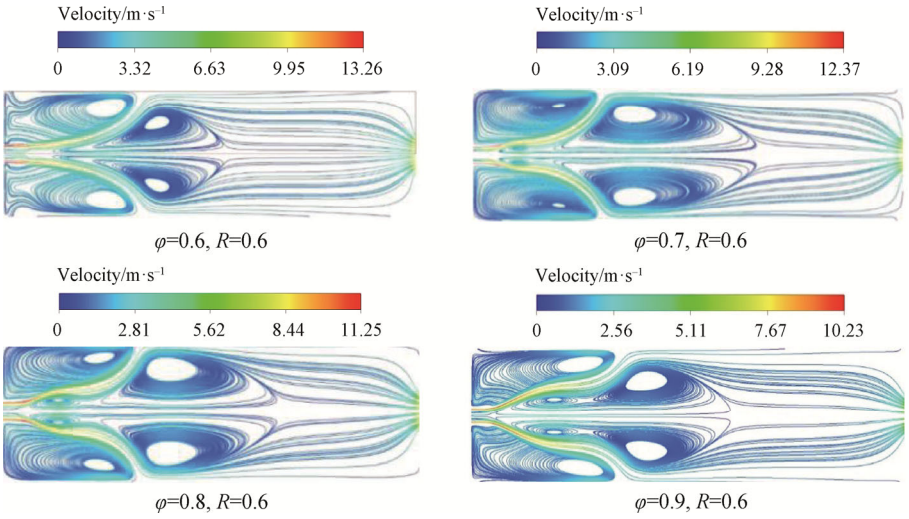

Fig. 8 The contour of streamlines at different stoichiometric ratios, R=0.6 and θ=35°

reduces the mixture of fresh reactants converted to hot products by flame, thereby reducing the production of pollutants. The flow enclosed between the wall and the outlet radiated flow is the same as the outer vortex. There is a significant temperature difference between this region and the inner vortex region.

In Fig. 9, the profile of axial temperature distribution at different equivalence ratios is shown. Here, as the fuel-to-air ratio increases, the position of the maximum flame temperature moves downstream. With increasing fuel-to-air ratio, the maximum temperature also increases, so that at φ=0.6, the maximum temperature in the position x=0.3l is equal to 1473 K. Increasing the equivalence ratio to φ=0.9, the maximum temperature occurs in x=0.2l, equal to 1973 K. As the equivalence ratio increases, the enthalpy of the reactants and consequently the flame temperature increase, too. The lower the flame temperature is, the lower the amount of produced pollutants is, indicating that a stable flame in the mixture in a low-swirl burner leads to the flame with low temperature with dilute fuel. The results are consistent with Periagaram's research [47].

Fig. 10 shows the axial velocity profile in four different equivalence ratios. The results reveal that the axial velocity decreases when the fuel-air mixture exits due to the radial flow. This decrease leads to flow reversal, the creation of circulation, and the formation of vortices. The velocity inside that area becomes negative, indicating that the velocity is in the opposite direction of the inlet flow. This turbulence applied to the flame increases the flame stability without reversal.

3.2 The effect of equivalence ratio at R=0.6 with θ=41°

When the cross-sectional area of the axial flow is 0.6 of the total cross-sectional area, and the swirling flow with θ=41° enters the burner, the problem is analyzed in φ=0.6, 0.7, 0.8, and 0.9. Fig. 11 and Fig. 12 show the contours of velocity distribution and streamlines in four different equivalence ratios, respectively. Here, two vortices are formed by the swirl of the premixed flow, the central part of which has only an axial velocity due to the swirl of the flow near the wall. The swirling flow causes

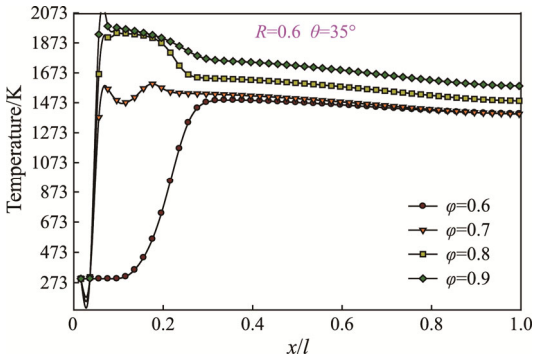

Fig. 9 Axial temperature distribution at different equivalence ratios, R=0.6 and θ=35°

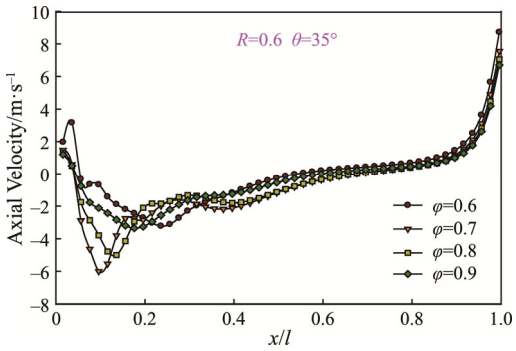

Fig. 10 Axial velocity distribution at different equivalence ratios, R=0.6 θ=35°

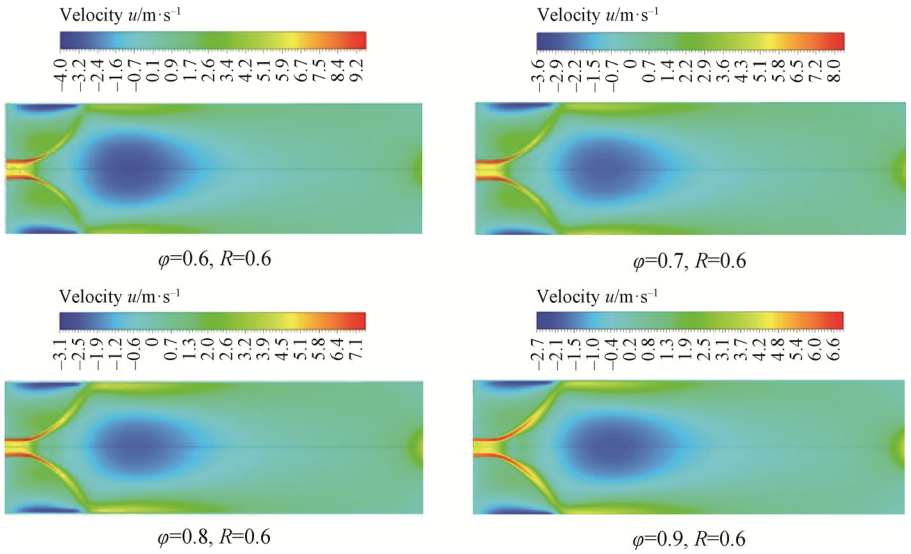

Fig. 11 The contour plot of axial velocity distribution at different equivalence ratios, R=0.6 and θ=41°

the axial flow to diverge by applying the radial velocity component. The shear flow formed by the interaction of the axial and radial flows leads to the formation of a pair of vortices on the axis, a pair of vortices behind the shear line. Analysis of the effect of equivalence ratio on maximum axial velocity shows that increasing the equivalence ratio leads to decreasing axial velocity. At φ=0.6, the maximum axial velocity is 9.2 m/s; at φ=0.9, this value is 6.6 m/s. Reduction in the axial velocity increases the detention time of the products and the number of pollutant species. Thus, the production of pollutants can be reduced using the appropriate equivalence ratio, leading to an increase in axial velocity.

Fig. 13 and Fig. 14 show the temperature and fourth power distribution contours to investigate the trend and flame shape. As shown in Fig. 13, as the equivalence ratio increases, the maximum temperature increases from 1460 K to 2047 K, and the temperature of the vortex behind the shear flow and the walls (outer vortex) is lower than that of the flow inside the shear flow. It is possible to analyze the shape of the flame by the distribution of the fourth power of temperature in Fig. 14. Here, as the fuel-to-air ratio increases, the flame structure changes so that at φ=0.9, the divergence angle increases considerably, and the flame is formed as a narrow V-shaped band. Increasing the equivalence ratio at a constant fuel flow rate is associated with a decrease in air, thereby increasing the flame temperature in the combustion chamber. Fig. 15 shows the distribution of CO_2 along the axis at the minimum and maximum equivalence ratios to investigate the effect of the equivalence ratio on the production of pollutants in combustion products. Here, after the exit of the fuel-air mixture, the mass fraction of CO_2 is the maximum at

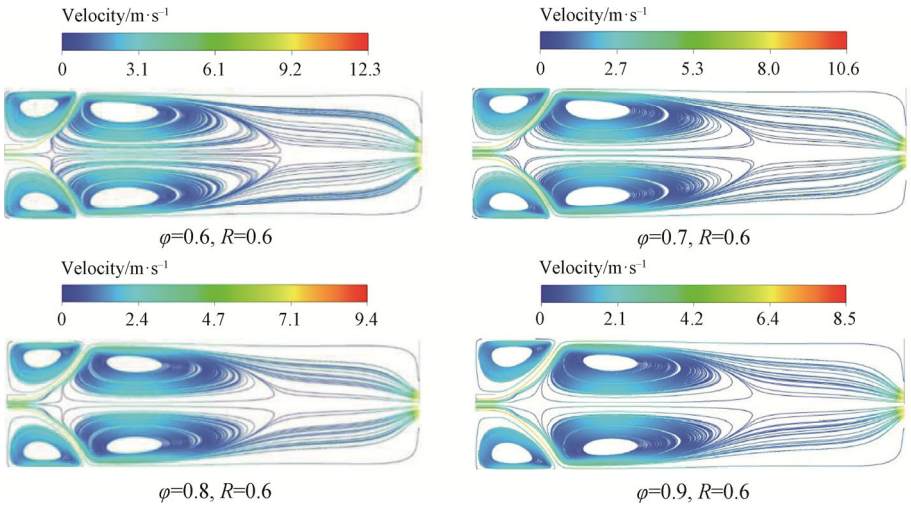

Fig. 12 The contours of streamlines at different equivalence ratios, R=0.6 and θ=41°

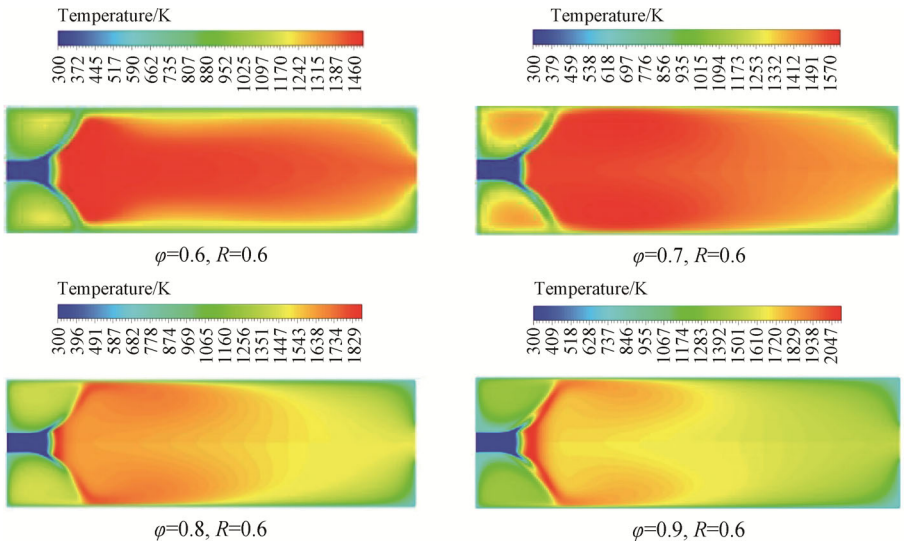

Fig. 13 The contours of temperature distribution at different equivalence ratios, R=0.6 and θ=41°

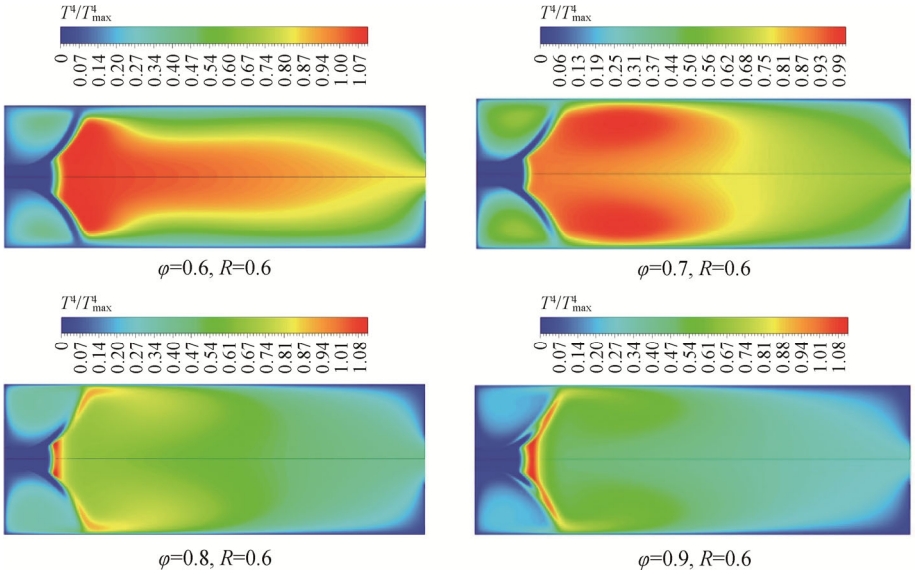

Fig. 14 The contours of the distribution of fourth power temperature (flame shape) at different equivalence ratios, R=0.6 and θ=41°

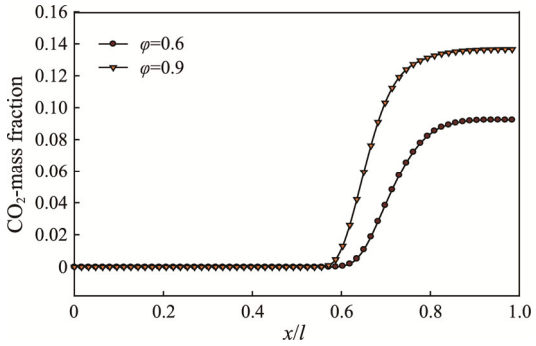

Fig. 15 Mass fraction of CO_2 along with the chamber at different equivalence ratios and θ=41°

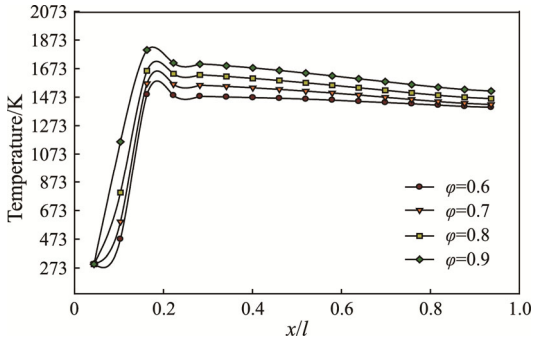

Fig. 16 The profile of temperature distribution along the axis at different equivalence ratios, R=0.6 and θ=41°

the position where the flame temperature is maximum. As shown in Fig. 15, as the equivalence ratio increases from φ=0.6 to 0.9, the maximum mass fraction of CO_2 in the combustion chamber increases from 0.08 to 0.14. A quantitative analysis of the changes in temperature and velocity in the combustion chamber is presented.

Fig. 16 shows the axial temperature distribution when the θ=41° and the ratio of the axial radius to the total inlet radius are 0.6. Here, increasing the equivalence ratio has a significant effect on temperature changes. By changing φ from 0.6 to 0.7 after reaching the maximum temperature value, the flame temperature along the axis does not decrease significantly, and the flame is emitted in the axial direction. However, when φ=0.8 and 0.9, the axis temperature reaches a maximum value, and then the flame temperature decreases along the axis, indicating that as the equivalence ratio increases, the length of the flame decreases. This axial temperature distribution is consistent with the temperature distribution contours shown in Figs. 13 and 14. Results show that the maximum flame temperature also increases so that in φ=0.6, the maximum temperature is equal to 1463 K and the maximum temperature when φ=0.9 is equal to 2083 K. Considering the V-shape flame, the temperature along the axis of the burner decreases to 1583 K.

Fig. 17 shows the axial velocity profile along the burner axis when φ=0.6, 0.7, 0.8, and 0.9. Here, after the exit of the fuel-air mixture, the axial velocity decreases linearly due to the presence of a radial velocity resulting from the swirling flow, leading to the radial propagation of the flow and reduction in axial velocity. The reduction in axial velocity changes its direction, leading to the formation of a vortex. As the distance from the entry point of the swirling flow increases, the axial velocity is amplified again, and its value becomes positive. As shown in Fig. 17, as the equivalence ratio increases from φ=0.6 to 0.9, the velocity in the centre of the vortex x=0.3l increases from –3.8 m/s to –2 m/s.

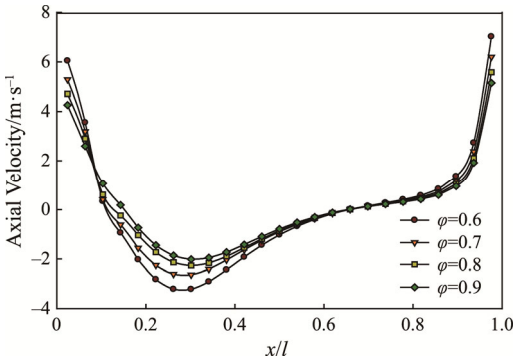

Fig. 17 The axial velocity profile along the axis at different equivalence ratios, R=0.6 and swirl angle of 41°

3.3 Effect of equivalence ratio at R=0.6 with θ=47°

The flow's behaviour and shape are analyzed when the swirling flow enters the burner with θ=47° from the wall. Fig. 18 shows the contour of axial velocity when R=0.6. Here, at θ=47° swirl angle of the fuel-air mixture outlet at all equivalence ratios is V-shaped, and the flame divergence is observed using its velocity distribution. As shown in Fig. 18, when φ=0.6, the maximum axial velocity is 9.1 m/s, and the minimum velocity in the areas where the vortex is formed as –4 m/s. By increasing the equivalence ratio to φ=0.9, the maximum axial velocity reaches 6.9 m/s.

Fig. 19 shows the contour of streamlines when R=0.6. Here, at this relatively high swirl angle, the high-power swirling flow has adequately affected the axial component of the flow, and the flow has also propagated in the radial direction, leading to the formation of a vortex. As shown in Fig. 19, by increasing the equivalence ratio in a constant fuel flow, the air share in the mixture practically decreases. The velocity value decreases so that in the flow with φ=0.6, the maximum velocity is 11.8 m/s. Inflow with φ=0.9, this value is reduced to 8.27 m/s. Reduction in velocity increases the detention time of the products and the number of pollutant species. Stable flame combustion at a low fuel-to-air ratio is one of the advantages of low swirl flames.

Figs. 20 and 21 show the fourth temperature power (flame shape) and temperature contours, respectively. Here, with increasing the equivalence ratio, the shape of the flame and the maximum temperature of the combustion chamber change significantly, so that in φ=0.6 and φ=0.7, the flame is stretched throughout the burner, and the maximum temperature is equal to 1472 K; however, when φ=0.9, the flame is completely divergent and is mainly formed at the outlet of the air-fuel mixture, and the maximum temperature increases to 2063 K.

Fig. 22 shows the axial temperature distribution in φ=0.6, 0.7, 0.8 and 0.9 when θ=47°. Here, at φ=0.6, after the fuel-air mixture is ignited and the flame is formed, the maximum temperature reaches around 1483 K, and as it moves along the length of the combustion chamber, the temperature does not decrease. This temperature distribution indicates that at φ=0.6, the flame divergence is insufficient, and the flame is formed by stretching in the combustion chamber. Analysis of the temperature distribution by approaching the stoichiometric Ratio 1 (ideal conditions) shows that as the fuel-air mixture thickens (increasing the equivalence ratio), the profile of axial temperature changes, so that in φ=0.9, after leaving the inlet duct, the temperature of the fuel-air mixture reaches its maximum value, which is equal to 2128 K and then the axial temperature decreases along with the chamber, indicating that with increasing fuel-to-air ratio,

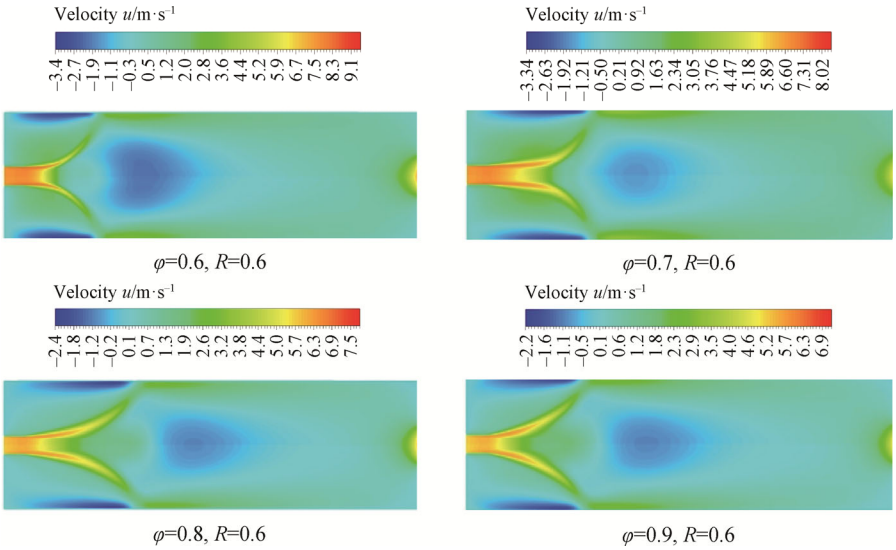

Fig. 18 The contour of axial velocity distribution at different equivalence ratios, R=0.6 and θ=47°

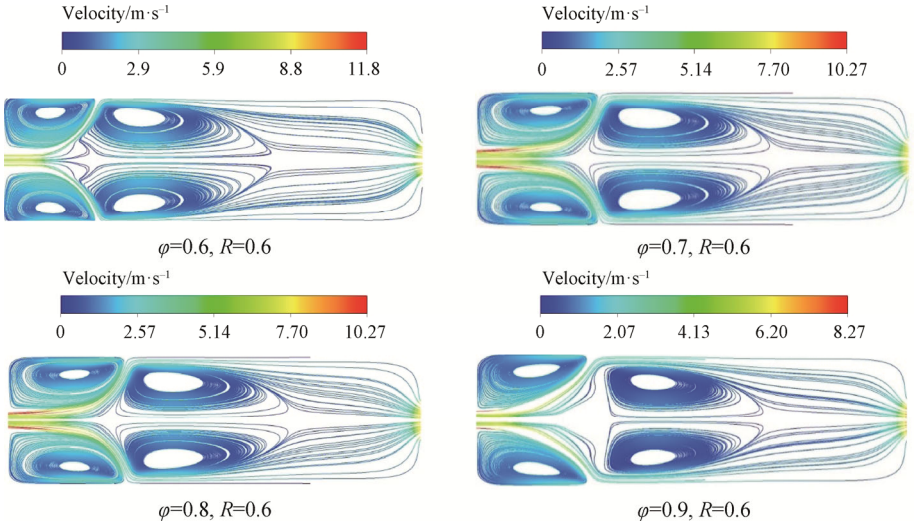

Fig. 19 The contour of streamlines, at different equivalence ratios, R=0.6 and θ=47°

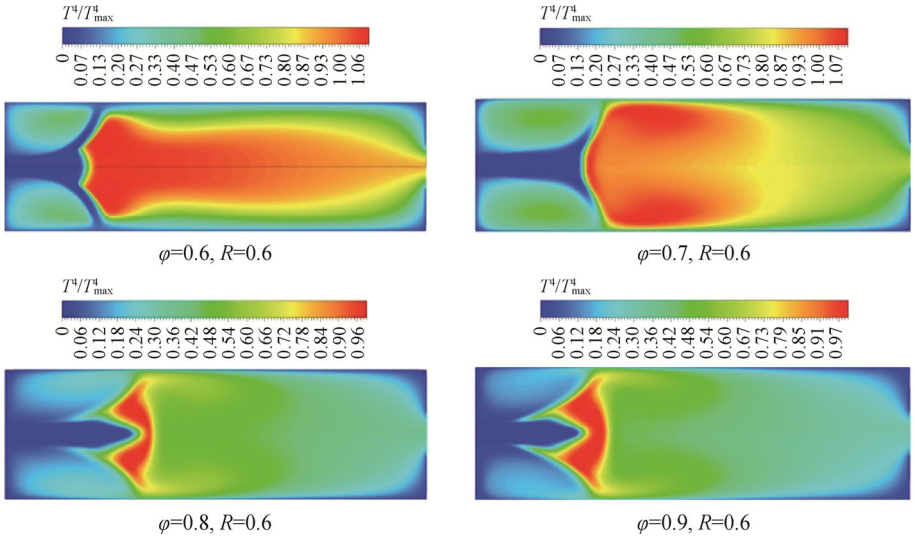

Fig. 20 The contours of the distribution of fourth power temperature (flame shape) at different equivalence ratios, R=0.6 and θ=47°

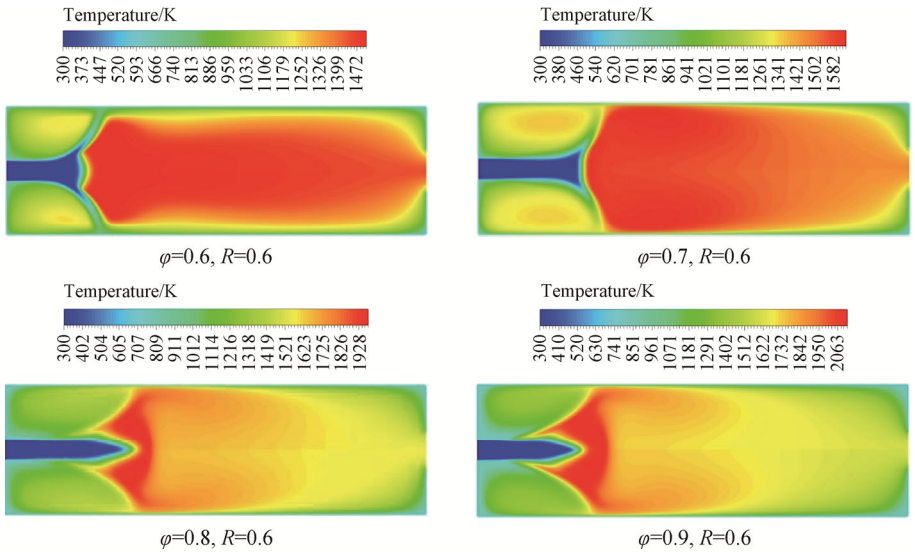

Fig. 21 The contour of temperature distribution at different equivalence ratios, R=0.6, θ=47°

the flame tends toward the outlet of the fuel-air mixture. The swirling flow significantly affects divergence and prevents the propagation of the flame (high-temperature range) throughout the chamber.

Fig. 23 shows the axial velocity in the combustion chamber. At φ=0.6, the flame is stretched in the combustion chamber. Analysis of the changes in axial velocity shows that in this stoichiometric ratio, the velocity is opposite the x-axis and the length of the formed vortex is more than other conditions examined. As shown in Fig. 21, at φ=0.6, the velocity in the opposite direction of the flow at the center of the vortex is –2 m/s, while at φ=0.9, this value decreases to –1 m/s. Therefore, by increasing the fuel-air ratio, the axial velocity is amplified, and the radial flow in some areas close to the outlet section of the fuel-air mixture affects the flow field.

Fig. 24 shows the distribution of CO_2 as one of the combustion pollutants in two minimum and maximum stoichiometric ratios. Here, with increasing the fuel-air ratio, the mass fraction of CO_2 increases to 0.14.

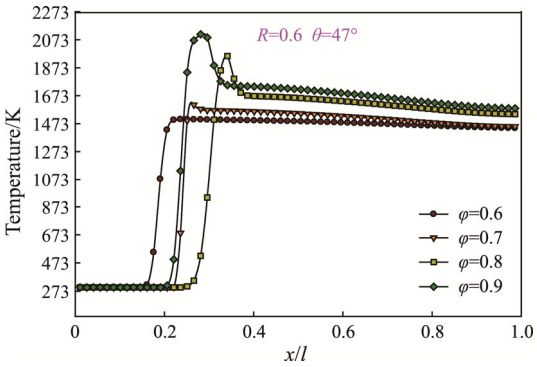

Fig. 22 The axial temperature profile at different equivalence ratios, R=0.6 and θ=47°

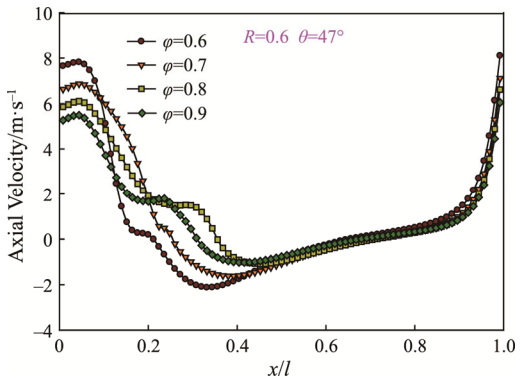

Fig. 23 The axial velocity profile at different equivalence ratios, R=0.6 and θ=47°

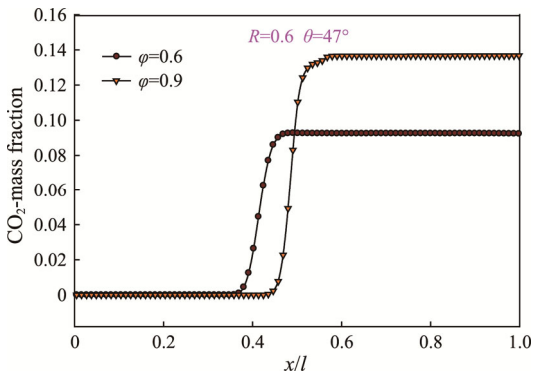

Fig. 24 The profile of mass fraction distribution of CO_2 at different equivalence ratios, R=0.6 and θ=47°

3.4 Effect of flow swirl angle at φ=0.9 and R=0.6

Fig. 25 shows the axial temperature distribution when the swirling flow is affected by three different angles of θ=35°, 41°, and 47°. Here, with increasing the swirl angle, the maximum temperature of the combustion chamber is affected. As the swirl angle increases, the maximum flame temperature moves away from the inlet of the fuel-air mixture, and its value also increases. The results indicate in the swirling flow with θ=35°, the maximum temperature occurs in the position x=0.08l, however, in the swirl angle with θ=41°, this position reaches x=0.12l. Moreover, the analysis of the maximum temperature of the combustion chamber shows that at θ=35°, the maximum temperature is 1984 K, and at θ=41°, this value reaches 2085 K. Also, Fig. 25 shows that by increasing the swirl angle to θ=47°, the position of the maximum flame temperature is found at a considerable distance from the fuel and air inlet, and its value in the position x=0.3l is equal to 2115 K. The distance between the position of the maximum temperature and the burner minimizes the damage to the burner wall. The maximum temperature and its position depend on the flame's shape, the flow physics, and the mixing intensity of the fuel-air mixture. The results reveal that by increasing the swirl angle applied to the flow, the mixing intensity and flow turbulence increase, increasing the flame temperature and the temperature of the combustion chamber.

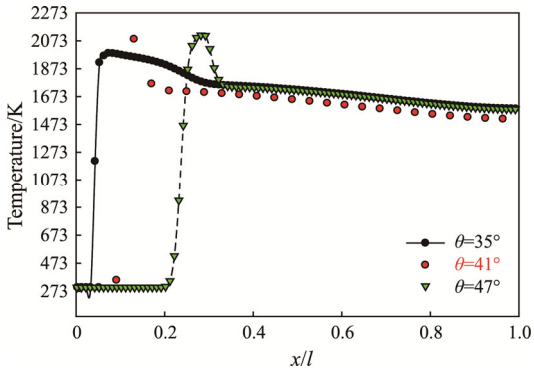

Fig. 25 The temperature profile along the axis at different swirl angles, at φ=0.9

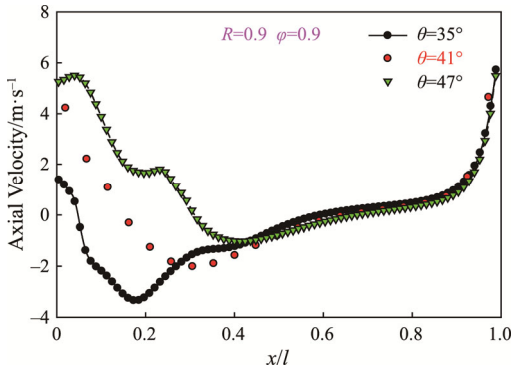

Fig. 26 The axial velocity profile along the axis at different swirl angles, at φ=0.9, R=0.6

Fig. 26 shows the axial velocity of the combustion chamber when the swirling flow is affected by three different angles of θ=35°, 41°, and 47°. Here, as the swirl angle increases, the position of the minimum velocity value (in the opposite direction of the axis) tends toward the outlet, indicating that with increasing the swirl angle, its effect on velocity divergence increases, and the axial velocity is affected by the radial velocity due to the swirling flow. In addition to the position of the minimum velocity, the minimum velocity value also decreases with increasing swirl angle.

3.5 The effect of equivalence ratio at R=0.65 with θ=41°

Fig. 27 shows axial velocity contours at φ=0.6, 0.7, 0.8 and 0.9. Here, with increasing the equivalence ratio, the axial velocity is affected, so that its value in φ=0.9 is 6.6 m/s, however, at the equivalence ratio φ=0.6, the maximum axial velocity value is 9.5 m/s, indicating that by increasing the fuel-air ratio, the radial velocity applied by the swirling flow at a higher equivalence ratio has a higher effect on the axial velocity divergence and a high effect on the axial velocity. Fig. 28 shows the contours of streamlines at φ=0.6, 0.7, 0.8 and 0.9. Here, the axial flow is affected by the radial flow, and a vortex is formed after the exit of the fuel-air mixture. Comparison of the length of the vortices shows that in combustion with φ=0.6, the vortices become more stretched, and with increasing fuel-air ratio, the vortices become shorter and weaker. The contours of streamlines and velocity indicate that the shapes of the flame in φ=0.6 and 0.7 become more stretched along the combustion chamber axis. However, with increasing fuel-air ratio, the flame stretch in the chamber is reduced, and the flame is well stretched in the radial direction, as shown in the temperature contours in Fig. 29.

Fig. 30 shows the temperature profile along the axis of the combustion chamber in four equivalence ratios when θ=41° and R=0.65. Here, with an increasing equivalence ratio, the combustion temperature increases due to the increase in the enthalpy of the reactants. Analysis of the temperature profile shows that its position also changes the maximum temperature value. With an increasing equivalence ratio, the centre of the flame approaches the outlet of the fuel-air mixture. Fig. 31 shows the axial velocity profile at φ=0.6, 0.7, 0.8 and 0.9. Here, in all four cases, the axial velocity is initially affected by the swirling flow, and as the axial flow diverges, its velocity decreases and even reaches a negative value. The negative value of axial velocity indicates circulation and the presence of vortices. The contours of the velocity and streamlines indicate the existence of these vortices that are formed by swirling flow. The axial flow is affected by the radial velocity caused by the swirling flow, and by increasing the equivalence ratio, the velocity decreases in

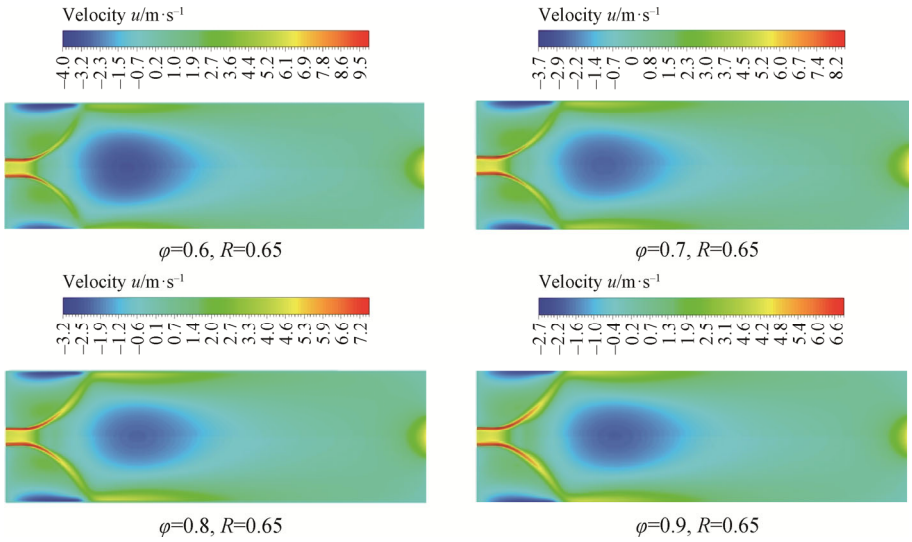

Fig. 27 The contour of axial velocity at different equivalence ratios, R=0.6 and θ=41°

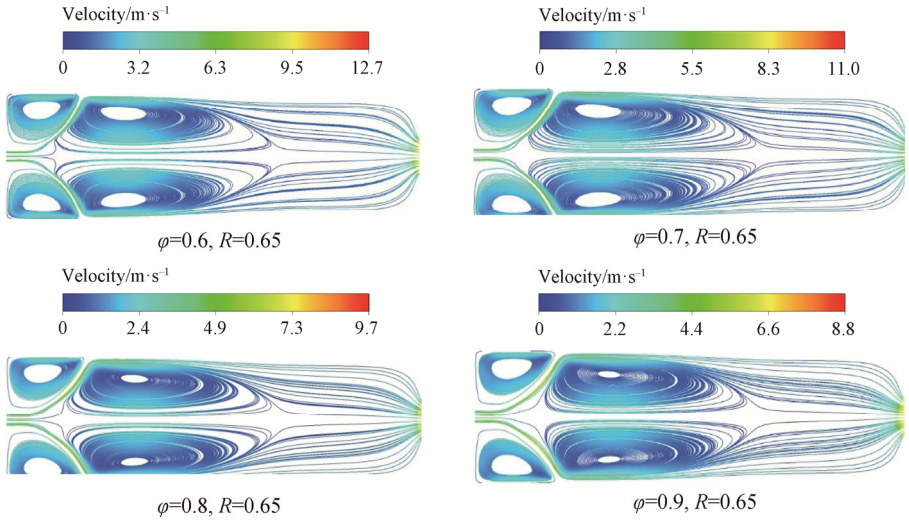

Fig. 28 The contour of streamlines at different equivalence ratios, R=0.65 and θ=41°

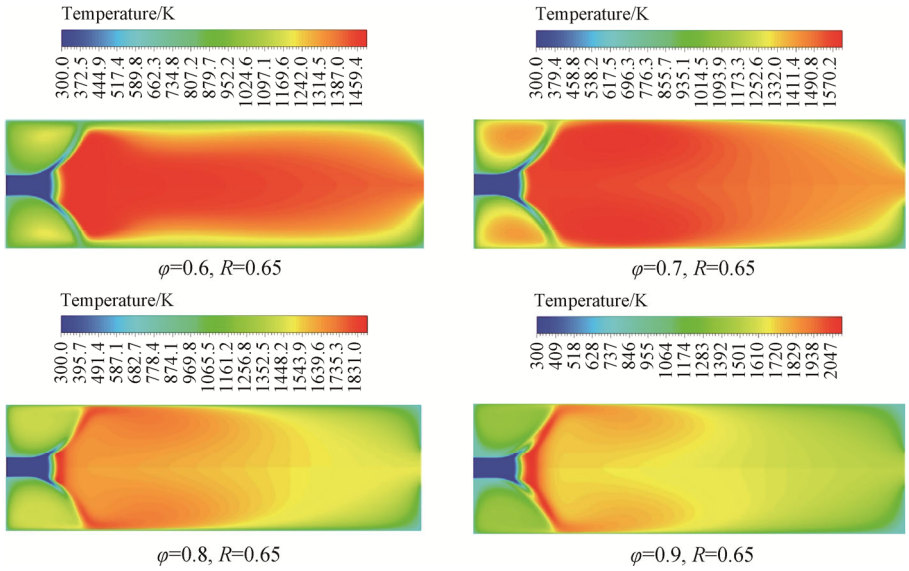

Fig. 29 The contour of temperature at different equivalence ratios, R=0.65 and θ=41°

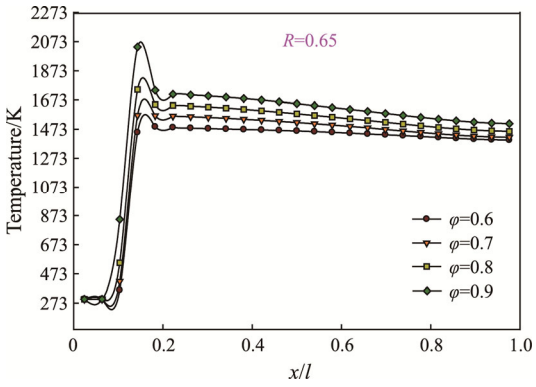

Fig. 30 The axial temperature profile at different equivalence ratios, R=0.65 and θ =41°

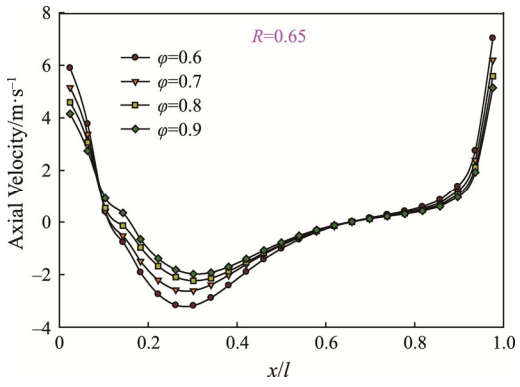

Fig. 31 The axial velocity profile at different equivalence ratios, R=0.65 and θ =41°

the opposite direction of the axial flow in the vortex core. As the radial flow enters the chamber, the radial velocity decreases, and the axial flow tends toward the outlet

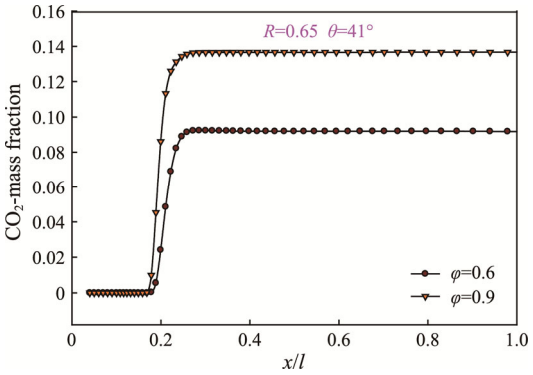

Fig. 32 The CO_2 distribution in the axial direction at different equivalence ratios, R=0.65 and θ =41°

chamber again. Fig. 32 shows the distribution of CO_2 as one of the products in the minimum and maximum fuel-air ratios. Here, with increasing fuel-air ratio, the production of this pollutant increases due to decreasing the axial velocity, increasing the flame temperature, and increasing the detention time of the products.

3.6 Effect of equivalence ratio at R=0.7 with θ=41°

In this section, the behaviour of flow and flame is analyzed at R=0.7 with θ=41°. Figs. 33 to Fig. 35 show the contours of temperature, streamlines, and axial velocity at φ=0.6, 0.7, 0.8, and 0.9, respectively.

The results reveal that due to the weakness of the radial velocity component, the vortex enclosed between the chamber wall and the shear flow resulting from the flow swirling propagates and affects the central vortex so that in φ=0.6, four vortices are formed in the axis of the

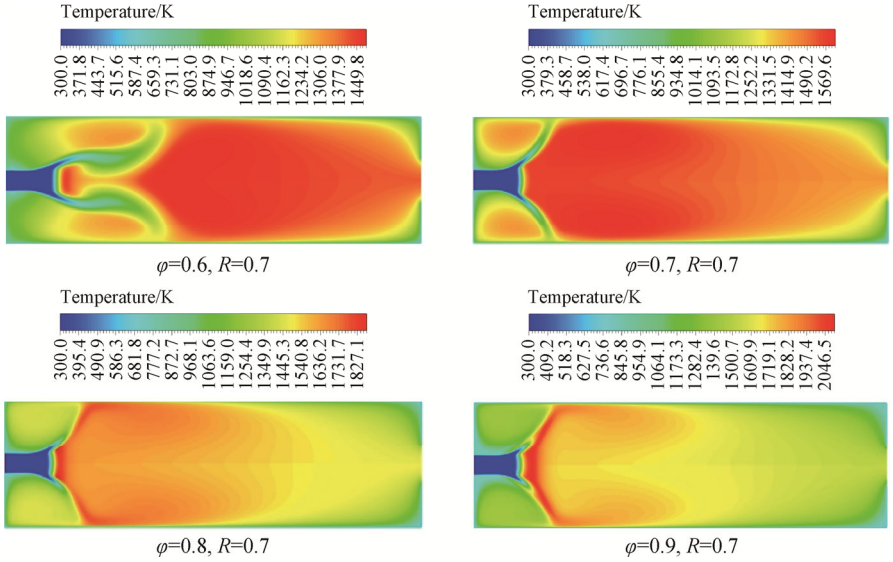

Fig. 33 The contours of temperature at different equivalence ratios, R=0.7 and θ=41°

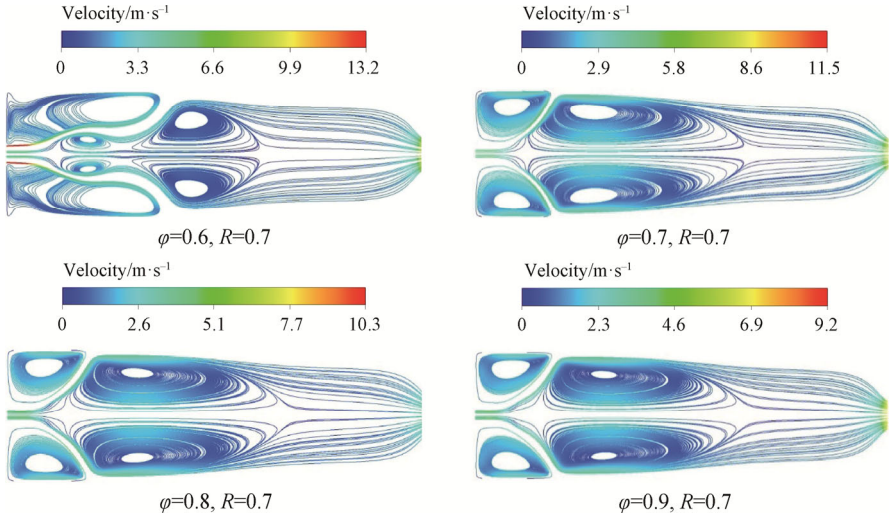

Fig. 34 The contours of streamlines at different equivalence ratios, R=0.7 and θ=41°

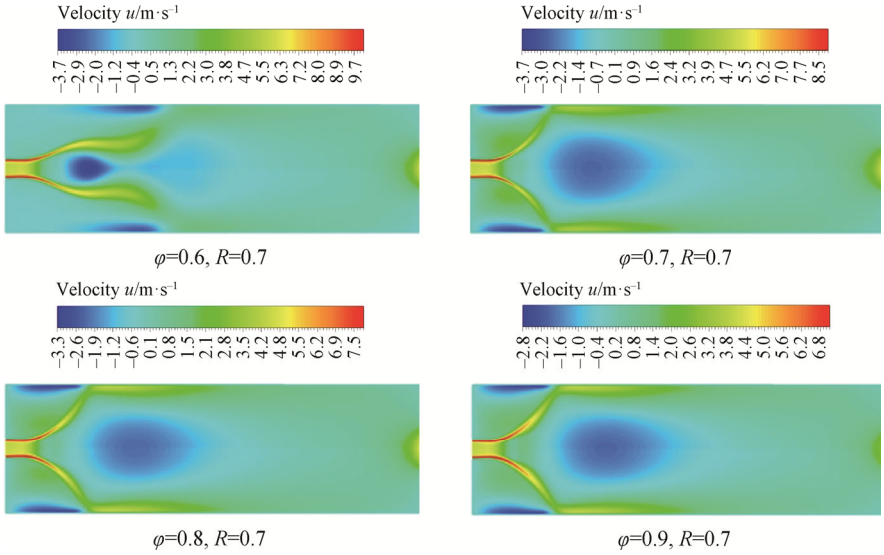

Fig. 35 The velocity contours at different equivalence ratios, R=0.7 and θ=41°

combustion chamber. However, increasing the equivalence ratio, the swirling flow forms the shear layer and affects the axial velocity. There is also a vortex between the wall and the shear flow. The contour plot of the temperature shows that with increasing the fuel-air ratio, the divergence angle reaches its maximum value and the flame length in the chamber decreases, and the maximum temperature also increases so that in φ = 0.6, the maximum temperature is 1449 K. In φ=0.9, it increases to 2046 K. Increasing the chamber's temperature leads to an increase in the production of pollutants, which is not desirable. The quantitative changes of velocity and temperature along the combustion chamber axis are quantitatively dealt with, too.

Fig. 36 shows the temperature profile along the combustion chamber axis at φ=0.6, 0.7, 0.8, and 0.9 when θ=41°. Here, with increasing equivalence ratio, the values of the maximum axial temperature of the combustion chamber and the outlet temperature increase. The results indicate that at φ=0.6, the maximum temperature is 1533 K, and at the chamber's outlet, the temperature is 1168 K. When φ=0.9, the maximum temperature is 2104 K, and the outlet temperature of the chamber is 1708 K. Therefore, with a 50% increase in fuel, the maximum temperature increases by 45% and the outlet temperature by 60%. The temperature of the combustion chamber increases as the equivalence ratio increases due to increasing the enthalpy of the reactants, which increases the amount of heat released and consequently the temperature of the chamber. Fig. 37 shows the axial velocity profiles along the combustion chamber axis at φ=0.6, 0.7, 0.8, and 0.9 when θ=41°. Here, in φ=0.6, the axial velocity changes are different from other analyzed conditions, which is also shown

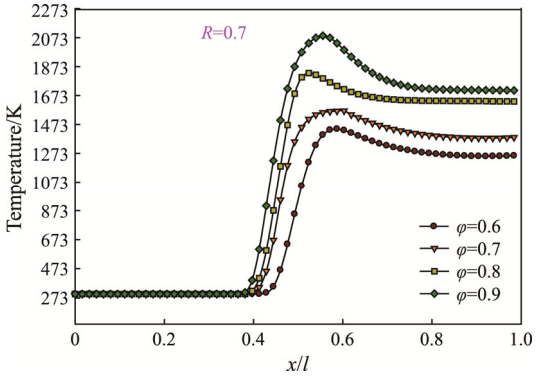

Fig. 36 The axial temperature profile at different equivalence ratios, R=0.7 and θ=41°

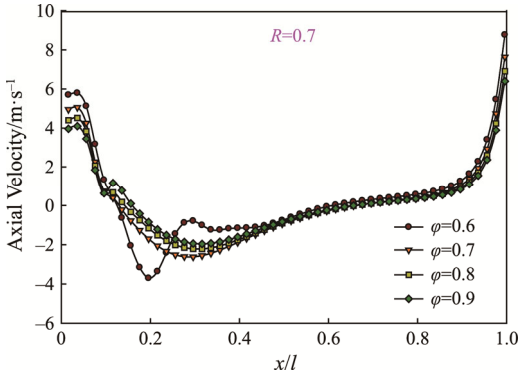

Fig. 37 The axial velocity profile at different equivalence ratios, R=0.7 and θ =41°

by analyzing the streamlines. In these conditions, the axial velocity decreases due to the radial velocity resulting from the swirling flows. Even its value reaches less than zero, indicating the existence of the circulation and a vortex. After the formation of the first vortex, the

axial velocity increases again. However, with the formation of the second vortex, the axial velocity decreases again. Moreover, at higher fuel-to-air ratios, after the axial flow velocity decreases and the vortex is formed, the effect of the swirling flow is eliminated, the axial velocity is recovered, and its value in the direction of the axis increase again.

Fig. 38 shows the distribution of CO_2 at φ=0.6 and φ=0.9. Here, with increasing the equivalence ratio, the mass fraction of CO_2 increases from 0.08 to 0.14. The increase in CO_2 occurs due to the increase in the fuel-air ratio resulting from increased combustion temperature.

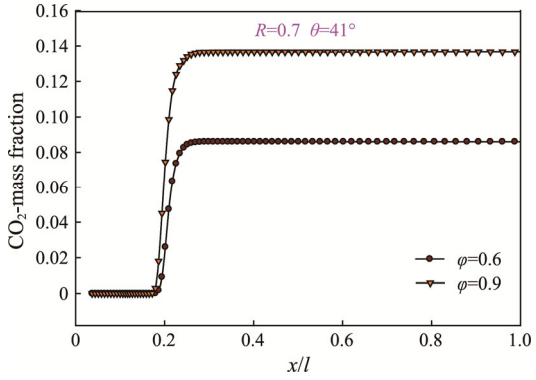

Fig. 38 The carbon dioxide distribution at different equivalence ratios, R=0.7 and θ=41°

By comparing the simulation results with the results of Adewole [48], Belal [49], Huang [50], and Sapra [51], it can be concluded that in these studies, parameters such as the effect of air to fuel ratio, rotation angle applied on the rotating blower on field characteristics, flow, temperature, and pollutant production have been investigated. In the present study, the effects of equivalence ratios and swirl angles of different flows and changing the inlet radius of the axial flow on the stability of the flame have been investigated, which is an innovation of this research.

4. Conclusion

In the present study, the combustion flow of methane gas in a low-swirl burner is simulated using a partially premixed combustion model. The accuracy of the obtained numerical results is evaluated by validation (Ebrahim et al. [43]). The results show that:

(1) In general, at φ=0.6, different swirl angles increase, the maximum flame temperature increases, and the maximum temperature tend toward the fuel-air mixture's outlet. Furthermore, the velocity and length of the flame in the axial direction decrease and the axial velocity in the internal vortices in the reverse axial direction reaches its minimum value.

(2) As the equivalence ratio increases, the maximum temperature of the flame increases, and its position tends towards the outlet of the fuel-air mixture.

(3) With increasing the equivalence ratio, the effect of radial velocity on the axial velocity decreases. The velocity in the centre of the vortex increases with an increasing fuel-to-air ratio.

(4) As the swirl angle increases, the maximum temperature position of the combustion chamber is affected, and the maximum flame temperature position moves away from the inlet of the fuel-air mixture, and its value also increases.

(5) As the swirl angle increases, the position of the minimum velocity value tends toward the outlet, indicating that with increasing the swirl angle, its effect on velocity divergence increases, and radial velocity affects the axial velocity.

(6) As the radius of the axial flow increases, the burner's temperature increases, and its position tends toward the outlet of the combustion chamber.

References

[1] Kotb A., et al., Case study for swirling flow and porous media on triple coaxial ports inverse diffusion flame. Alexandria Engineering Journal, 2022, 61(3): 2294–2306. DOI: 10.1016/j.aej.2021.07.017

[2] Liu V.W., Mohamad A., Kamal M., Pollution reduction from flares by swirl vanes in a cross-flow. International Journal of Environment and Pollution, 2007, 31(1–2): 193–209. DOI: 10.1504/ijep.2007.015675

[3] Ismael A., Abdelkhalek M., Kamal M., Combustion performance of eccentrically rotated flames. Proceedings of the Institution of Mechanical Engineers, Part A: Journal of Power and Energy, 2013, 227(5): 593–611. DOI: 10.1177/0957650913489295

[4] Elgamal G., Kamal M., Abdulaziz A., Swirl and cross-flow effects on vitiated jet flames. Combustion Science and Technology, 2013, 185(2): 310–335. DOI: 10.1080/00102202.2012.718007

[5] Leong K.A., The Effect of centerline enrichment for flexible low swirl burner flame stabilization. 2017, University of California, Irvine.

[6] Kamal M., Mohamad A., Effect of swirl on performance of foam porous medium burners. Combustion science and technology, 2006, 178(4): 729–761. DOI: 10.1080/00102200500248482

[7] Kashkousha O., Kamal M., Abdulaziz A., Nosier M., Inverse diffusion and partially premixed flames with elliptical/swirling-and cross-flows. Proceedings of the Institution of Mechanical Engineers, Part A: Journal of Power and Energy, 2015, 229(1): 44–59. DOI: 10.1177/0957650914552155

[8] Azam E., Kamal M.M., Abotaleb H.A., Combustion

performance of triple flames issuing from elliptical Swirlers. IOSR Journal of Engineering, 2016, 6(5): 34–47.

[9] Fahmy A., Abotaleb H., Kamal M., Combustion characteristics of inverse diffusion flames with elliptic swirlers. IOSR Journal of Engineering, 2016, 6(4): 27–44.

[10] Mohy M., Saad H., Kamal M., Effect of the degree of ellipticity on the combustion performance using Elliptic double swirlers. IOSR Journal of Engineering, 2016, 6: 13–21.

[11] Cheng R.K., Low swirl combustion. The Gas Turbine Handbook, 2006, pp. 241–255.

[12] Frank A., Therkelsen P., Sierra A.M., Rapp V.H., Cheng R.K., Chen J.-Y., Investigation of the down-scaling effects on the low swirl burner and its application to microturbines. in: Turbo Expo: Power for Land, Sea, and Air, American Society of Mechanical Engineers, 2018, pp. V04BT04A062.

[13] Cheng R., Yegian D., Miyasato M., Samuelsen G., Benson C., Pellizzari R., Loftus P., Scaling and development of low-swirl burners for low-emission furnaces and boilers. Proceedings of the Combustion Institute, 2000, 28: 1305–1313.

[14] Zhao Y., Shao W., Liu Y., Tang X., Xiao Y., McDonell V., Numerical and experimental study of geometry effects on fuel/air mixing and combustion characteristics of a dln burner. in: ASME Power Conference, American Society of Mechanical Engineers, 2020, pp. V001T003A004.

[15] Ter Linden A., Investigations into cyclone dust collectors, Proceedings of the Institution of Mechanical Engineers. 1949, 160: 233–251.

[16] Beér J.M., Combustion aerodynamics, in: Combustion Technology, Elsevier, 1974, pp. 61–89.

[17] Claypole T., Syred N., Effect of swirl burner aerodynamics on NO_x/formation. United States, Cardiff University, Cardiff, Wales, 1981.

[18] Buckley P., Craig R., Davis D., Schwartzkopf K., The design and combustion performance of practical swirlers for integral rocket/ramjets. AIAA Journal, 1983, 21: 733–740.

[19] Cho E.-S., Chung S.H., Improvement of flame stability and NO_x reduction in hydrogen-added ultra lean premixed combustion. Journal of Mechanical Science and Technology, 2009, 23: 650–658.

[20] Tummers M., Hübner A., Van Veen E., Hanjalić K., Van der Meer T.H., Hysteresis and transition in swirling nonpremixed flames. Combustion and Flame, 2009, 123: 447–459.

[21] Zhao Z., Yuen D., Leung C.W., Wong T., Thermal performance of a premixed impinging circular flame jet array with induced-swirl. Applied Thermal Engineering, 2009, 23: 159–166.

[22] Paubel X., Cessou A., Honore D., Vervisch L., Tsiava R., A flame stability diagram for piloted non-premixed oxycombustion of low calorific residual gases. Proceedings of the Combustion Institute, 2007, 31: 3385–3392.

[23] Hashemi S.A., Nikfar M., Motaghedifard R., Experimental study of operating range and radiation efficiency of a metal porous burner. Thermal science, 2015, 19: 11–20.

[24] Li J., Zhao H., Study of premixed flame stabilization by using opposed jet. Science in China Series E: Technological Sciences, 1998, 41: 76–81.

[25] Ciani A., Kreutner W., Hubschmid W., Frouzakis C., Boulouchos K., Experimental investigation of the morphology and stability of diffusion and edge flames in an opposed jet burner. Combustion and Flame, 2007, 150: 188–200.

[26] Raghavan V., Experimental study of pre-mixed flames on a multi-hole matrix burner. International Journal of Integrated Engineering, 2012, 4(1): 1–5.

[27] Kerr N., Swirl effect on flame performance and the modeling of the swirling flames. Journal of the Institute of Fuel, 1965, 38: 527–538.

[28] Mathur M., Maccallum N., Swirling air tests issuing from vane swirlers. Journal of the Institute of Fuel, 1976, 41: 238–240.

[29] Yuasa S., Effects of swirl on the stability of jet diffusion flames. Combustion and Flame, 1986, 66: 181–192.

[30] Gupta A.K., Lilley D.G., Syred N., Swirl flows, Tunbridge Wells, 1984.

[31] Feikema D., Chen R.-H., Driscoll J.F., Enhancement of flame blowout limits by the use of swirl. Combustion and Flame, 1990, 80: 183–195.

[32] Choi B.-C., Kim H.-T., Flame stability of CO/H_2 syngas in the diffusion flame by using lab-scale burner. Environmental Engineering Research, 2003, 8: 193–201.

[33] Cavaliere D.E., Kariuki J., Mastorakos E., A comparison of the blow-off behaviour of swirl-stabilized premixed, non-premixed and spray flames. Flow, Turbulence and Combustion, 2013, 91: 347–372.

[34] Heeger C., Gordon R., Tummers M., Sattelmayer T., Dreizler A., Experimental analysis of flashback in lean premixed swirling flames: upstream flame propagation. Experiments in Fluids, 2010, 49: 853–863.

[35] Kwark J.-H., Jeong Y.-K., Jeon C.-H., Chang Y.-J., Effect of swirl intensity on the flow and combustion of a turbulent non-premixed flat flame. Flow, Turbulence and Combustion, 2005, 73: 231–257.

[36] Kotani Y., Takeno T., An experimental study on stability and combustion characteristics of an excess enthalpy flame. Symposium (International) on Combustion, 1982, 19(1): 1503–1509.

[37] Chao Y.-C., Wu C.-Y., Lee K.-Y., Li Y.-H., Chen R.-H., Cheng T.-S., Effects of dilution on blowout limits of

turbulent jet flames. Combustion Science and Technology, 2004, 173: 1735–1753.

[38] Lee P.H., Lee J.Y., Han S.S., Park C.S., Hwang S.S., Formation of lean premixed flat flame using cylindrical porous metal plate burner. in: Proceedings of the fourth European Combustion Meeting Vienna, Austria, Citeseer, 2009.

[39] Diamantis D., Mastorakos E., Goussis D., Simulations of premixed combustion in porous media. Combustion Theory and Modelling, 2002, 6: 383.

[40] Hashemi S.A., Amani J., Atoof H., Experimental study of flame stability in SiC Porous Media. Amirkabir Journal of Science and Technology, 2011.

[41] Hashemi S., Kolak H., Aghaei A., Experimental Study of Premixed Flames Stabilization with Al_2O_3 Porous Media. Amirkabir Journal of Mechanical Engineering, 2017, 49: 625–634.

[42] Lee S., Kum S.-M., Lee C.-E., Performances of a heat exchanger and pilot boiler for the development of a condensing gas boiler. Energy, 2011, 36: 3945–3951.

[43] Feyz M.E., Esfahani J., Pishbin I., Razavi S.M., Effect of recess length on the flame parameters and combustion performance of a low swirl burner, Applied Thermal Engineering, 2015, 89: 609–617.

[44] Jones W., Whitelaw J., Calculation methods for reacting turbulent flows: a review. Combustion and Flame, 1982, 48: 1–26.

[45] Cellek M.S., Turbulent flames investigation of methane and syngas fuels with the perspective of near-wall treatment models. International Journal of Hydrogen Energy, 2020, 45: 35223–35234.

[46] Cellek M.S., Flameless combustion investigation of CH_4/H_2 in the laboratory-scaled furnace. International Journal of Hydrogen Energy, 2020, 45: 35208–35222.

[47] Periagaram K.B., Determination of flame characteristics in a low swirl burner at gas turbine conditions through reaction zone imaging. Georgia Institute of Technology, 2012.

[48] Adewole B.Z., Abidakun O.A., Asere A.A., Artificial neural network prediction of exhaust emissions and flame temperature in LPG (liquefied petroleum gas) fueled low swirl burner. Energy, 2013, 61: 606–611.

[49] Huang L., Liu C., Deng T., Jiang H., Wu P., Experimental investigation on the influence of central airflow on swirl combustion stability and flame shape. Journal of Thermal Analysis and Calorimetry, 2021, 144: 503–514.

[50] Sapra G., Chander S., Effect of operating and geometrical parameters of tangential entry type dual swirling flame burner on impingement heat transfer. Applied Thermal Engineering, 2020, 188: 115936.